Relative Permeability Measurement Using Rapid In-Situ Saturation Measurement with ^{23}Na MRI

Mohammad Sadegh Zamiri[1], *Naser* Ansaribaranghar[1,2], *Florea* Marica[1], *Andrés* Ramírez Aguilera[1], *Derrick* Green[3], *Cyril* Caubit[4], *Benjamin* Nicot[4], and *Bruce J.* Balcom[1,*]

[1]UNB MRI Research Centre, Physics Department, University of New Brunswick, Fredericton, NB E3B 5A3, Canada
[2]Department of Chemical Engineering, University of New Brunswick, Fredericton, NB E3B 5A3, Canada
[3]Green Imaging Technologies, Fredericton, New Brunswick E3A 8V2, Canada
[4]TotalEnergies, Pau, France

Abstract. Relative permeability (k_r) curves are essential for reservoir management. Commonly, SCAL techniques for estimation of k_r curves rely on laboratory core flood experiments. During these experiments, temporal data such as volume of produced fluid and pressure drop across the core plug, are used to evaluate k_r curves as a function of water saturation, S_w. Laboratory infidelities, in particular the capillary end effect, prevent direct application of Darcy's law for k_r measurements. Therefore, the analysis of temporal data relies on simulations to separate capillary pressure (P_c) effects from relative permeability. These simulations can predict the results of a core flood experiment by using $P_c(S_w)$ and $k_r(S_w)$ as input functions. Therefore, the inverse problem is solved by assuming parametrized functional forms for $P_c(S_w)$ and $k_r(S_w)$. The temporal data is then fit by optimizing these parameters to obtain P_c and k_r curves. Magnetic resonance imaging (MRI) can be used to monitor the core flood experiment to provide temporal and spatial fluid saturations during a core flood experiment. Rapid in-situ saturation monitoring using MRI can be used to give derivatives of saturation with respect to time and position. In this work, a technique is proposed that employs saturation derivatives as well as the pressure drop across a core plug to extract model-free k_r curves. To validate the proposed method, the core analysis simulation program CYDAR was used to generate saturation profiles as well as the pressure drop across the core plug for drainage and imbibition processes, assuming P_c and k_r curves. These data were then used in the proposed method to retrieve the k_r curves. To showcase the validity of the method experimentally, a drainage experiment was conducted to evaluate k_r curves in a Bentheimer core plug undergoing first drainage.

1 Introduction

An important part of laboratory special core analysis (SCAL) is measurement of relative permeability (k_r) curves. These curves are of vital importance in reservoir simulations. Reservoir development plans whether for petroleum production or storage of hazardous materials are based on analysis of these reservoir simulations and economic factors. k_r curves have a direct impact on production and injection forecasts of the reservoir simulations. Therefore, they significantly influence reservoir management decisions [1, 2].

k_r curves are empirical parameters that correct Darcy's law for multiphase flow in porous media. They are function of fluid saturation and distribution of phases [2-5]. Therefore, k_r curves integrate wettability and displacement mechanism information into the reservoir simulation. Robust methodologies for measuring k_r curves are essential for ensuring the accuracy and reliability of reservoir simulations, ultimately contributing to the successful management and exploitation of hydrocarbon reservoirs.

Capillary effects, namely the capillary end effect occur in laboratory core flood experiments, preventing direct application of Darcy's law for k_r measurement [6]. Additionally, it is important to have a consistent set of k_r and P_c curves representing displacement experiments. Therefore, it is essential to measure capillary pressure and relative permeability curves simultaneously in one displacement experiment [7]. However, this presents challenges due to the large number of unknown parameters defining k_r and P_c curves. These parameters are commonly fitted to limited measured quantities. Commonly, the measured quantities in a core flooding experiments are pressure drop across the core plug and production data [8-10]. In-situ saturation monitoring is increasingly available in core analysis laboratories. However, this additional data has usually been used to further constrain the optimization algorithms [7, 11-13].

There is a wealth of methodologies to derive relative permeability curves reported in the literature [12, 14-17]. The common feature of these methods is that they use core

* Corresponding author: bjb@unb.ca

flood numerical simulations to fit results of displacement experiments [17, 18]. These simulations can predict experiment outcomes if capillary pressure and relative permeability curves are available. This process is known as forward simulation. However, determining capillary pressure and relative permeability curves requires solving an inverse problem, which is inherently ill-posed due to the excessive number of unknowns. To mitigate this, parametrized functional forms are employed for capillary pressure and relative permeability as functions of fluid saturations [17, 19, 20]. These parameters are subsequently optimized to fit the experimental dataset and derive the desired curves.

Goodfield et al. [21] proposed a methodology for deriving relative permeability curves using in-situ saturation data. In their analysis, the pressure drop equation was oversimplified, leading to inaccurate relative permeability functions. More significantly, the proposed methodology was not tested experimentally. In this work, we use the proposed method coupled with the correct pressure equation to derive relative permeability curves. In this work, it is shown that model assumption of relative permeability curves can be discarded using in situ saturation data. A common functional model for relative permeability curves is Corey's model [19]. It is known that complex pore structures as found in rocks with vug pores can result in non-Corey type relative permeability curves [22]. In such cases, an analysis method that does not rely on a predetermined functional form for relative permeability curves becomes essential.

In the current work, in-situ saturation data and pressure drop across the core plug are employed to calculate relative permeability curves. The methodology is first tested using synthetic core flooding data, generated using a core flooding numerical simulation software for a drainage and an imbibition scenario. To generate the synthetic data, relative permeability and capillary pressure curves were assumed. The numerical simulation software was then used to generate the pressure drop across the core plug and saturation data. This data was then used in the proposed methodology to re-generate the relative permeability and capillary pressure curves. A drainage experiment was conducted on a water-wet Bentheimer sandstone.

In-situ saturation data was measured using ^{23}Na magnetic resonance imaging (MRI). Application of ^{23}Na MRI allows acquisition of high-resolution saturation profiles without the need to resolve the MRI signal for oil and water [23, 24].

Application this method offers a model-free measurement of relative permeability curves, that can play an important role in prediction of petroleum production from oil and gas reservoirs.

2 Theory and Methodology

2.1 Background

The two-phase Darcy equation is used to model a one-dimensional displacement of two immiscible fluids in a core plug [25].

$$q_\alpha = -\frac{\beta \mathrm{K} A k_{r\alpha}}{\mu_\alpha}\frac{\partial P_\alpha}{\partial x} \tag{1}$$

Equation 1 relates flow rate, q to pressure drop along the flow direction, $\frac{\partial P}{\partial x}$. α stands for oil and water phase. The proportionality constant in Eq. 1 consists of absolute permeability of the porous media, K, cross sectional area, A, dynamic viscosity, μ of phase α, and relative permeability of phase α, $k_{r\alpha}(S_\alpha)$ which is a function of fluid saturation, S_α. β is a unit conversion factor. The continuity equation ensures the conservation of mass during the displacement, and it is represented using Eq. 2.

$$\frac{\partial q_\alpha}{\partial x} = -\phi A \frac{\partial S_\alpha}{\partial t} \tag{2}$$

where ϕ is the porosity of the core plug. To complete the two-phase flow formulation, several auxiliary relations, Eqs. 3-5 a consequence of the presence of two phases in the core plug, are also required.

$$q_t = q_o + q_w \tag{3}$$

$$P_c(\mathrm{S}_w) = P_o - P_w \tag{4}$$

$$S_o + S_w = 1 \tag{5}$$

where q_t represents total flow rate, assuming incompressible fluids, P_c stands for capillary pressure and difference in pressure of oil and water phases. Defining fluid mobility $\lambda_\alpha = \frac{K.k_{r\alpha}}{\mu_\alpha}$, fractional flow of water, f_w, and capillary dispersion, $D_c(S_w)$ [26],

$$f_o(S_w) = \frac{\lambda_o}{\lambda_w + \lambda_o} \tag{6}$$

$$D_C(S_w) = -\beta A \lambda_w f_o(S_w)\frac{\partial P_c}{\partial S_w} \tag{7}$$

and combining Eqs. 1 and 2 gives a partial differential equation, Eq. 8, that describes the evolution of saturation in time and space for a two-phase flow problem.

$$\frac{\partial}{\partial x}\left(D_c(S_w)\frac{\partial S_w}{\partial x}\right) - q_t \frac{\partial f_w}{\partial S_w}\frac{\partial \mathrm{S_w}}{\partial x} = \phi A \frac{\partial S_w}{\partial t} \tag{8}$$

Solution of Eq. 8 requires boundary conditions. In a core flooding experiment, the boundary condition at the outlet end is zero capillary pressure. Therefore, the saturation at the effluent is $S_w(P_c = 0)$. The saturation at the inlet is discussed in the literature [27, 28]. In-situ saturation monitoring methods cannot capture the saturation at the very edges of a core plug. Therefore, direct application of Eq. 8 has not been possible.

2.2 Saturation Equation During Unsteady-State Fluid Injection

Goodfield et al. [21] proposed application of Eq. 2 to substitute the right side of Eq. 8 with $\frac{\partial q_w}{\partial x}$ and then integrating with respect to position to give:

$$\frac{q_w}{q_t} = f_w(S_w) + \frac{1}{q_t} D_C(S_w) \frac{\partial \mathrm{S_w}}{\partial x} \tag{9}$$

Equation 9 allows finding fractional flow of water, $f_w(S_w)$, and capillary dispersion, $D_c(S_w)$ without knowledge of boundary conditions. For a given saturation, S_w, Eq. 9 is a linear relationship between $\frac{1}{q_t}\frac{\partial \mathrm{S_w}}{\partial x}$ and $\frac{q_w}{q_t}$, with the slope of $D_C(S_w)$ and intercept of $f_w(S_w)$. q_w as a function of time, t and position, x can be calculated using Eq. 10 [21].

$$q_w(x,t) = q_w(x=0,t) - \phi A \int_0^x \frac{\partial \mathrm{S_w}(x',t)}{\partial t} dx' \tag{10}$$

2.3 Saturation Equation During Steady-State Fluid Injection

At steady-state conditions, the flow rate in time and space is equal to the injection flow rate, $q_w = q_t$. Therefore, Eq. 9 simplifies to show that $\frac{\partial \mathrm{S_w}}{\partial x}$ is directly proportional to the imposed flow rate, with a proportionality constant that is a function of saturation and is equal to $U(S_w)$.

$$q_t = \frac{D_C(S_w)}{1 - f_w(S_w)} \frac{\partial \mathrm{S_w}}{\partial x} \tag{11}$$

$$U(S_w) = \frac{D_C(S_w)}{1 - f_w(S_w)}$$

2.4 Pressure Equation

Combining Eqs. 1 and 2 for oil and water, and applying Eq. 4 to express water pressure as oil pressure leads to Eq. 12 and 13 [29]:

$$\frac{\partial}{\partial x}\left(\frac{\mathrm{KA}k_{ro}}{\mu_\mathrm{o}} \frac{\partial P_o}{\partial x}\right) = -\phi \mathrm{A} \frac{\partial S_o}{\partial t} \tag{12}$$

$$\frac{\partial}{\partial x}\left(\frac{\mathrm{KA}k_{rw}}{\mu_\mathrm{w}} \frac{\partial P_o}{\partial x} - \frac{\mathrm{KA}k_{rw}}{\mu_\mathrm{w}} \frac{\partial P_c}{\partial x}\right) = -\phi \mathrm{A} \frac{\partial S_w}{\partial t} \tag{13}$$

Adding Eqs. 12 and 13 eliminates saturations and gives an ordinary differential equation for oil pressure.

$$\frac{\partial}{\partial x}\left(\frac{\mathrm{KA}k_{ro}}{\mu_\mathrm{o}} \frac{\partial P_o}{\partial x}\right) + \frac{\partial}{\partial x}\left(\frac{\mathrm{KA}k_{rw}}{\mu_\mathrm{w}} \frac{\partial P_o}{\partial x} - \frac{\mathrm{KA}k_{rw}}{\mu_\mathrm{w}} \frac{\partial P_c}{\partial x}\right) = -q_{iw} - q_{io} \tag{14}$$

where $q_{i\alpha}$ is production or injection rate of phase α. The linearized form of the pressure equation, Eq. 14 is given in Appendix A. With known relative permeability curves, capillary pressure curves, and saturation profiles, the terms $k_{r\alpha}$ and P_c in Eq. 14 can be determined. By solving the linearized form of Eq. 14, pressure profiles can be obtained. Subsequently, the pressure drop across the core plug can be calculated based on the pressure profiles.

2.5 Parametrized Functions for Capillary Pressure Curve

Logbeta functions [17] were used to describe the capillary pressure as a function of water saturation. This function for the primary drainage case, water-wet P_c, is given in Eq. 15, and for an imbibition process where sample is partially oil wet is given in Eq. 16.

$$P_c(S_w) = -p_o \ln S_r + p_t \tag{15}$$

where p_t is the threshold pressure describing the pressure entry of the core for the oil phase, and S_r is the reduced water saturation given by Eq. 17.

$$P_c(S_w) = -a.p_o \ln \frac{1 - S_r^\beta}{S_r^\beta} - b \tag{16}$$

where $S_r^{P_c=0} = \left(\frac{1}{1+\beta}\right)^{1/\beta}$ is the reduced saturation at which P_c is zero, and $a = S_r^{P_c=0}(1 - S_r^{P_c=0})/\beta$, and $b = aP_o \ln \frac{1-\left(S_r^{P_c=0}\right)^\beta}{\left(S_r^{P_c=0}\right)^\beta}$.

$$S_r = \frac{S_w - S_{min}}{S_{max} - S_{min}} \tag{17}$$

For the primary drainage, S_{max} is 1, and the P_c function has three parameters: S_{min}, p_o, and p_t. For imbibition, the P_c function has four parameters: S_{min}, S_{max}, β, and p_o.

2.6 Methodology

The workflow to derive relative permeability curves from experimental data involves following the 5 steps. Saturation profiles and pressure drop across the core plug are the experimental data used in this methodology.

1. Derivative of saturation with respect to position, $Sx(x,t) = \frac{\partial \mathrm{S_w}}{\partial x}$ and time, $St(x,t) = \frac{\partial \mathrm{S_w}}{\partial t}$ are calculated.
2. $St(x,t)$ is used in Eq. 10 to obtain $q_w(x,t)$.
3. Fractional flow of water, $f_w(S_w)$, and capillary dispersion, $D_c(S_w)$ are calculated using Eq. 9.
4. A parametrized function for capillary pressure curve is assumed, which is then used to calculate $\frac{\partial P_c}{\partial S_w}$.
5. This step involves the inverse problem of finding the capillary pressure parameters that match the pressure drop data. Assuming the capillary pressure parameters, Eqs. 7 and 8 give a set of relative permeability curves. The relative permeability curves and the capillary pressure curve are used in the pressure equation, Eq. 14 to

give pressure drop across the core plug. The parameters of capillary pressure curve are then optimized to match the pressure drop across the core plug.

3 Experimental Section

A primary drainage experiment was conducted to test the ability of the method to extract relative permeability curves.

3.1 Rock and fluid properties

A core plug from a slab of Bentheimer sandstone was used for this experiment. The gravimetric porosity of the core plug was measured to be 0.24 p.u. using brine solution of 50 g/L NaCl. The absolute permeability of the core plug was measured 1.1 Darcy using brine. During the first drainage experiment S20 oil was injected into the core plug. Table 1 summarizes the rock and fluid properties.

Table 1. Rock and fluid properties for the first drainage experiment

Rock	L [cm]	D [cm]	ϕ [p.u.]	K [D]	μ_w [cp]	μ_o [cp]
Bentheimer	5.06	3.75	0.24	1.1	1	36.9

3.2 Core Flooding Instrument and Flooding Procedure

Figure 1 shows the core flooding flow diagram. Two pharmacia pumps (CYDAREX, Kercabellec, France) were used to inject oil and water to the sample. A separator (CYDAREX, Kercabellec, France) recycles both oil and water from the effluent to ensure continuous injection to the sample. The separator was also equipped with a level reading that allowed measurement of fluid production that was recorded using a TC08 USB data acquisition unit (OMEGA Engineering, Connecticut, USA). The same data acquisition unit was also used to read and record the data from a differential pressure transducer (OMEGA Engineering, Connecticut, USA) that measured pressure drop across the sample. A Quizix pump (Chandler Engineering, Oklahoma, USA) was used to pressurize the confining fluid in the coreholder to 15 bars.

The core plug was initially washed with alcohol and toluene using a Soxhlet instrument to ensure a water-wet sample. The sample was then saturated with the brine solution in a vacuum chamber. The sample was then placed in the MRI compatible coreholder fabricated from PEEK (TOTALEnergies, France). The absolute permeability was measured using brine.

3.3 MR instrumentation

A cryogen free variable field superconducting magnet (MR Solutions, Guildford, Surrey, UK) was used at a static magnetic field of 2.99 T to detect sodium-23. This magnetic field corresponds to a resonance frequency of 33.7 MHz for ^{23}Na which is solely present in the brine solution. The RF probe was a homemade birdcage. The magnet was permanently connected to a magnet power supply (Cryomagnetics, Inc., TN, US). GIT systems software (Green Imaging Technologies, Inc., NB, Canada) was employed to execute MR measurements. A shielded three axis gradient coil driven by Techron (Elkhart, IN) 7782 gradient amplifiers, provided maximum magnetic field gradients of 26 G/cm, 24 G/cm and 33 G/cm in x, y, and z directions, respectively.

3.4 MR methods and Parameters

Saturation profiles were acquired using the Spin Echo Single Point Imaging (SE-SPI) method. The SE-SPI method is capable of acquiring quantitative saturation profiles with minimal blurring [30, 31].

The 1D SE-SPI images had 64 pixels in a field of view of 70 mm, giving a nominal pixel size of 1.09 mm. The imaging measurement started with a 90° pulse length of 40 μs followed by a spatial encoding gradient of maximum of 5.27 G/cm and step size of 0.17 G/cm. 180° pulse length of 80 μs produced an echo 5 ms from the 90° pulse. The number of points acquired at the echo peak was 64. The imaging measurement required 13 mins with 16 signal averages and 9 echoes. Only the first echo was used to construct the image.

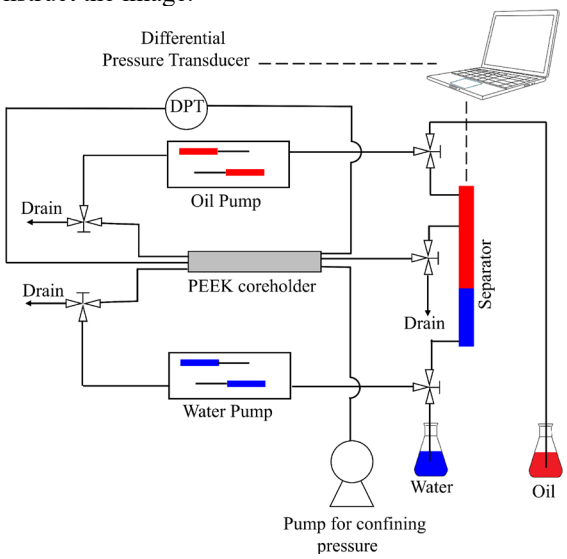

Fig. 1. Core flooding setup allowing for continuous injection of phases into the core plug. Pressure drop across the core plug and production data was recorded. The PEEK coreholder was positioned in the MRI instrument to measure fluid profiles with time.

4 Generated Data for Ground-Truth Cases

In this section, we report simulated imbibition and drainage displacements generated to give saturation profiles and pressure drop data. The core flooding simulation software, CYDAR was used to generate the ground-truth cases.

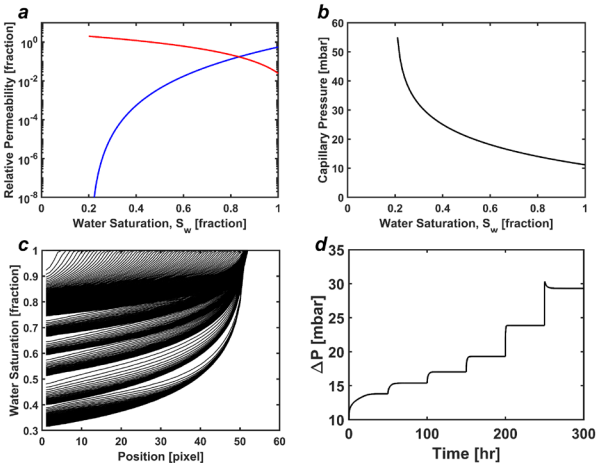

Fig. 2. Ground-truth drainage displacement case. (a) Relative permeability curves of water and oil phase defined based on Corey relationships given in Eqs, 18 and 19. Red and blue represent oil and water phases, respectively. (b) Capillary pressure curve defined using Eq. 15 with parameters given in Table 3. (c) Saturation profiles and (d) pressure drop were generated using CYDAR software.

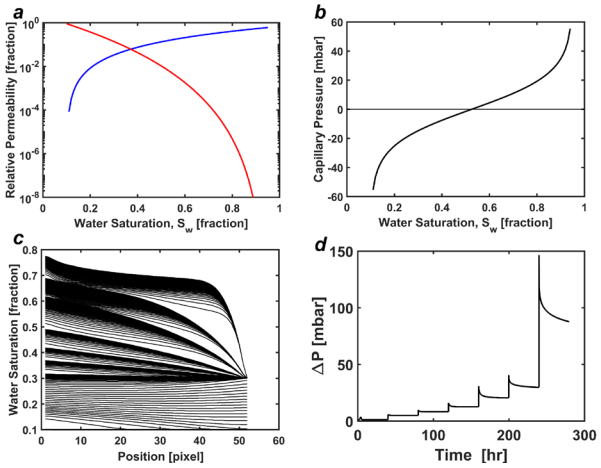

Fig. 3. Ground-truth imbibition displacement. (a) Relative permeability curves of water and oil phase defined based on Corey relationships given in Eqs, 18 and 19. Red and blue represent oil and water phases, respectively. (b) Capillary pressure curve defined using Eq. 16 with parameters given in Table 3. (c) Saturation profiles and (d) pressure drop were generated using CYDAR software.

4.1 Rock and fluid properties

Table 2 presents the rock and fluid properties used in the core flooding simulator to generate the saturation and pressure drop data for the imbibition and drainage process.

Table 2. Rock and fluid properties used for generating the ground truth cases

Process	L [cm]	D [cm]	ϕ [p.u.]	K [D]	μ_w [cp]	μ_o [cp]
Ground-truth simulation cases	5	3.81	0.24	1.6	1	32

4.2 Relative Permeability and Capillary Pressure Curves

Capillary pressure curves were defined using the Logbeta functions [17], given in Eqs. 15 and 16. Corey relationships, given by Eqs. 18 and 19, were used to define k_r curves [20]. The parameters for both relative permeability and capillary pressure curves are given in Table 3 for the imbibition and drainage cases. Figures 2a and 2b illustrate the defined curves for relative permeability and capillary pressure in the drainage scenario, while Figs. 3a and 3b depict those used in the imbibition scenario.

$$k_{rw} = k_{rw}^{max}\, S_r^{\alpha_w} \tag{18}$$

$$k_{ro} = k_{ro}^{max}\, (1 - S_r)^{\alpha_o} \tag{19}$$

Table 3. Parameters used to define relative permeability and capillary pressure curves for drainage and imbibition cases

Curves	Parameters	Imbibition	Drainage
Relative permeability parameters	k_{rw}^{max}	0.6	1
	k_{ro}^{max}	0.9	2
	α_w	2	5
	α_o	7	2
Reduced water saturation	S_{min}	0.1	0.2
	S_{max}	0.95	1
Capillary pressure parameters	p_o [mbar]	50	10
	p_t [mbar]	–	10
	β	1	–

Table 4. Flow rate bumps and their duration for the drainage and imbibition cases.

	Imbibition		Drainage	
Rate No.	Duration [hr]	Flow rate [ml/hr]	Duration [hr]	Flow rate [ml/hr]
1	40	0.6	50	0.12
2	40	3	50	0.3
3	40	6	50	0.6
4	40	12	50	1.2
5	40	30	50	3
6	40	60	50	6
7	40	300	–	–

The CYDAR software generated displacement data given in Fig. 2c and 2d for the drainage and Fig. 3c and 3d for the imbibition case. The orientation of displacement was horizontal. In the drainage scenario, the simulation involved injecting oil into rock that was originally saturated with brine. The oil was injected at constant flow rate conditions, with flow rate bumps specified in Table

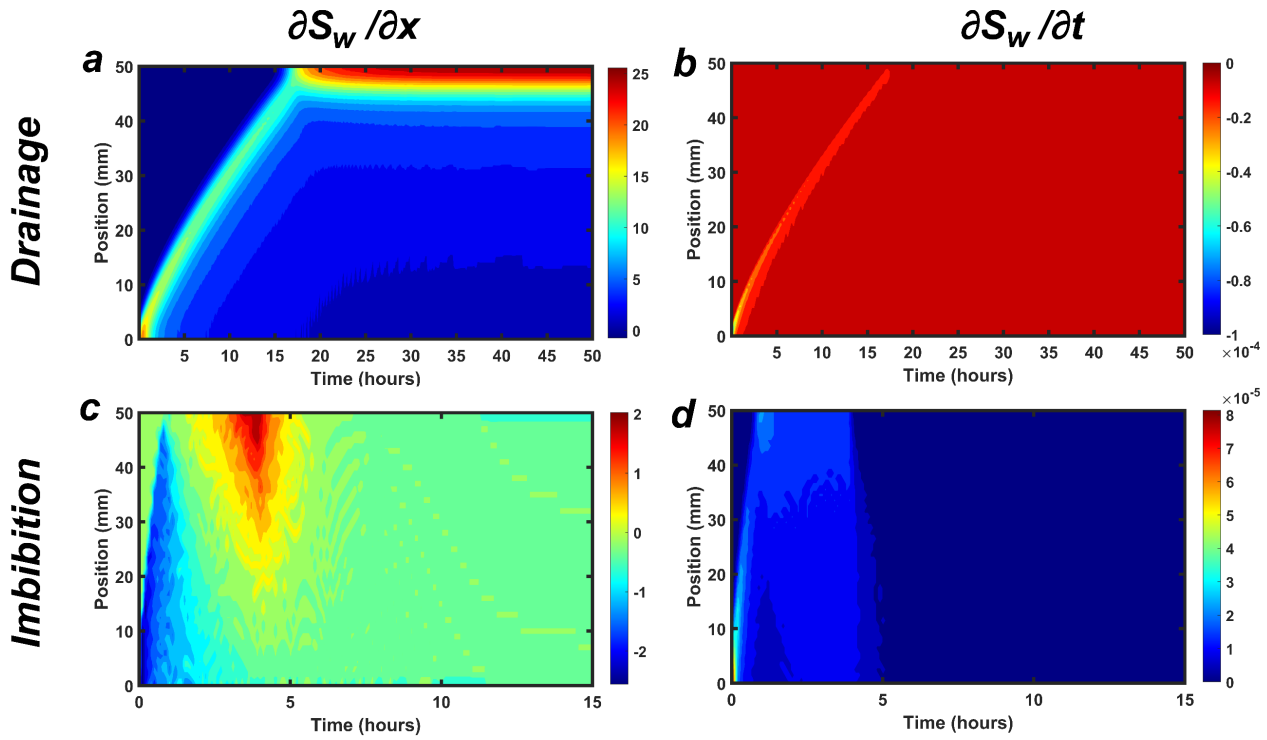

Fig. 4. Partial derivatives of water saturation for the first flow rate. Derivatives of water saturation with respect to position (a) and time (b) for the ground truth drainage case. Derivatives of water saturation with respect to position (c) and time (d) for the ground truth imbibition case.

4. In the imbibition case, water was injected into a rock that was initially at uniform irreducible water saturation of 0.1 s.u. (saturation units), at constant flow rate condition, with flow rate bumps given in Table 4.

Saturation data were generated using forward simulation in the CYDAR software with a 50-pixel resolution and with profiles captured at 7 min time intervals. Each bump flow rate was continued until steady-state condition was reached. Pressure drop data across the core plug was also generated using the numerical simulation software.

5 Implementation

The key element of the methodology is to first use the saturation data and its derivatives to find either two of the functions $f_w(S_w)$, $D_c(S_w)$, or $U(S_w)$. Then, optimize the $P_c(S_w)$ parameters to match the pressure drop data.

The first step is to calculate the derivatives of saturations. The ground-truth saturation profiles for the imbibition and the drainage cases, given in Figures 1 and 2, were used to calculate the derivatives of saturation with respect to time and position for the drainage and imbibition cases. The derivatives for the first flow rate are shown in Fiigure 4. Quantitative calculation of derivatives of saturation is crucial. The synthetic data used in this section was noise-free. Therefore, the derivatives are calculated with high fidelity. The front progression in the sample is evident in both the derivative of saturation with respect to time and position. $\frac{\partial S_w}{\partial t}$ approaches zero at the steady state, while

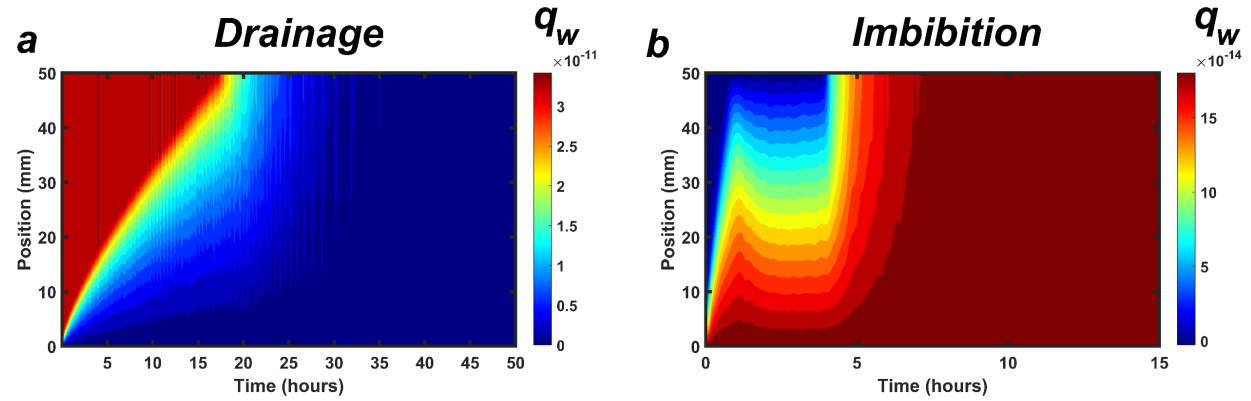

Fig. 5. Water flow rate in time and space shown for the first flow rate for the ground truth drainage (a) and imbibition (b) cases. Water low rate was calculated derivative of saturation with respect to time given in Fig. 4 and using Eq. 10.

$\frac{\partial S_w}{\partial x}$ reaches a steady state profile at the end of each flow rate.

Flow rate of water in time and space was calculated using Eq. 10, which uses the derivative of saturation with respect to time. The boundary condition, the first term in Eq. 10, was constant injection flow rate at the inlet. In the drainage case, the flow rate of water approaches zero, whereas, in the imbibition scenario, that matches the injection flow rate as the end of the process. The front movement is also evident in the flow rate maps. Quantitative calculation of flow rates depends of the accurate calculation of $\frac{\partial S_w}{\partial t}$.

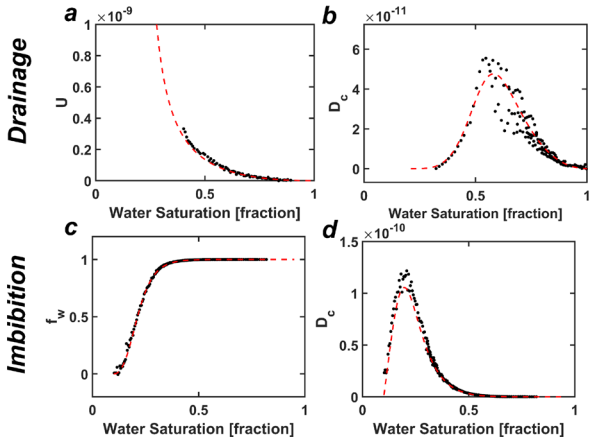

Fig. 6. Saturation-dependant functions, (a) $U(S_w)$ and (b) $D_c(S_w)$ calculated using Eq. 9 and 11 for the ground truth drainage case, employing derivative of saturation with respect to position and water flow rate. Saturation-dependant functions, (c) $f_w(S_w)$ and (d) $D_c(S_w)$ calculated using Eq. 9 for the ground truth imbibition case, employing derivative of saturation with respect to position and water flow rate. The dashed lines are the ground truth functions.

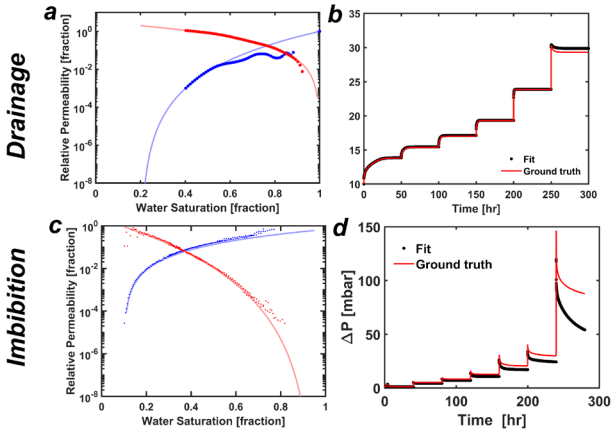

Fig. 7. (a) Relative permeability curves derived using the proposed method by fitting the pressure drop in (b) for the ground truth drainage case. (c) Relative permeability curves derived using the proposed method by fitting the pressure drop in (d) for the ground truth imbibition case. The continuous lines are the ground truth functions.

$f_w(S_w)$ and $D_c(S_w)$ can be obtained by tracking the unsteady-state saturation profiles with time and application of Eq. 9, while $U(S_w)$ is obtained using saturation profiles at the end of each flow rate bump and application of Eq. 11. Figure 6 presents the $f_w(S_w)$ and $D_c(S_w)$ for the imbibition case. In Figure 7, $U(S_w)$ and $D_c(S_w)$ are shown for the drainage case. The data points match the ground-truth curves that are known from the defined relative permeability and capillary pressure curves.

Saturation-dependant functions, $f_w(S_w)$, $D_c(S_w)$, and $U(S_w)$ as indicated in the Eqs. 6, 7, and 11, contain not only the relative permeability, but also the derivative of capillary pressure. To extract the relative permeability functions, parameterized capillary pressure curves were used. The parameters were then optimized using "patternsearch" function in MATLAB to match the pressure drop data. The optimized parameters are presented in Table 5. The resulting relative permeability curves and pressure drop fits for the imbibition and drainage cases are given in Figure 7.

Table 5. Fitted P_c parameters to match the pressure drop across the core plug for the ground truth imbibition and drainage cases.

	Reduced water saturation		Capillary pressure parameters	
Parameters	S_{min}	S_{max}	p_o [mbar]	β
Imbibition	0.1	0.90	10	1.05
Drainage	0.2	1	10	–

6 Results and Discussions

In this section, the drainage experiment described in the experimental section is analyzed to derive the relative permeability curves, employing two approaches: the method outlined in this study and the conventional numerical simulation method.

6.1 Proposed Method

Water saturation profiles acquired using ^{23}Na MRI using SE-SPI method are shown in Figure 8. The profiles show displacement of brine by the oil phase over time by imposing five flow rate bumps, specified in the caption of Figure 8. Higher flow rates allowed exploitation of relative permeability curves at lower water saturation. Derivatives of saturation and flow rate of water are calculated and shown in Figure 9.

Grouping data according to water saturation allowed the extraction of the saturation-dependent functions, $f_w(S_w)$ and $D_c(S_w)$. Each point in time and space defines a set of associated variables, $\{S, \partial S/\partial x, q_w\}$. These variable sets were organized based on a continuous increase in saturation values. The data was grouped into bins using 100 evenly distributed grid points in saturation. Subsequently, Eq. 9 was employed to create a linear relationship for each saturation, with f_w determined as the intercept of the line and D_c as its slope. The resulting $f_w(S_w)$ and $D_c(S_w)$ functions are shown in Figure 10. As per Eq. 7, $D_c(S_w)$ function includes derivative of capillary pressure. Therefore, to find relative permeability to oil and water phase at each saturation, knowledge of derivative of capillary pressure is required. To extract relative permeability curves, the capillary pressure functional form was selected according to the Eq. 15. The parameters of the

capillary pressure function were then optimized to fit the pressure drop data. The "patternsearch" function in MATLAB was used for the optimization.

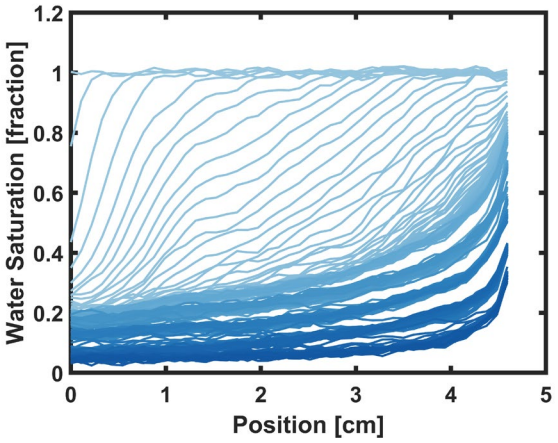

Fig. 8. Water saturation profiles acquired using ^{23}Na MRI for five oil flow rate bumps, 2, 4, 10, 30, and 60 ml/hr. Darker shades of blue represent higher injection flow rates.

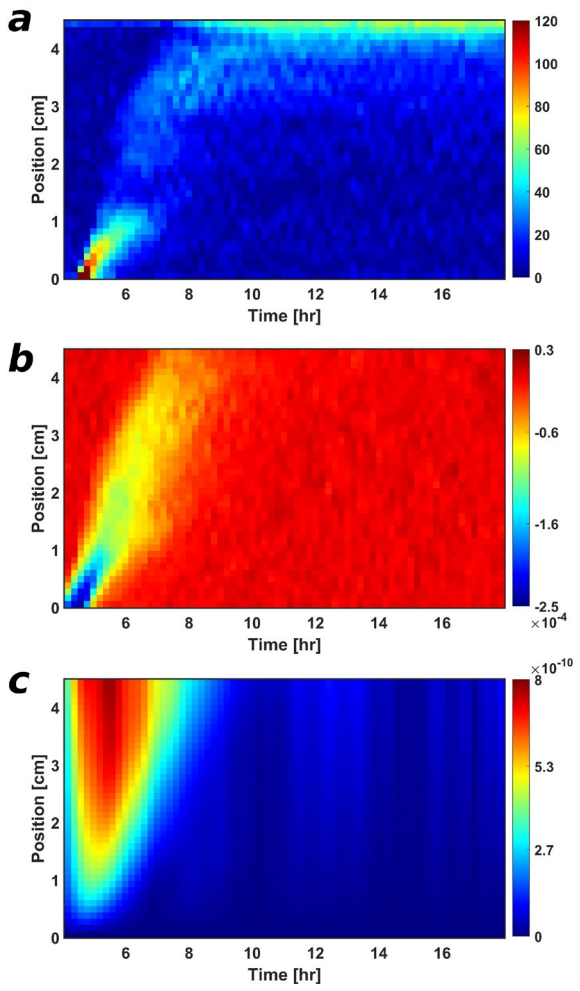

Fig. 9. Derivative of water saturation with respect to (a) position and (b) time, and (c) water flow rate map calculated using Eq. 10 for the oil first flow rate, 2 ml/hr.

The relative permeability curves extracted as a result of the optimization process are given in Figure 11a. The pressure drop, which was matched by tuning the capillary pressure parameters and solving the pressure equation (Eq. 14), is shown in Figure 11b in green. Table 6 presents the optimized parameters for capillary pressure curve.

6.2 Numerical Simulation

In this section, the conventional approach for deriving relative permeability curves was employed, which using CYDAR numerical simulation to match pressure drop across the sample and production data. The relative permeability curves were modeled using the Corey functions, given in Eqs.18 and 19. Eq. 15 was used for the capillary pressure curve. The CYDAR software optimized the parameters to match the pressure drop and production data. Figure 11a shows the relative permeability curves obtained using numerical simulation. The relative permeability curves using the proposed method (data points) agree with those from numerical simulation (continuous lines). Figure 11b and 11c illustrate the matched pressure drop and production data, respectively, in red using CYDAR. Table 6 presents the optimized parameters for relative permeability and capillary pressure curves by CYDAR.

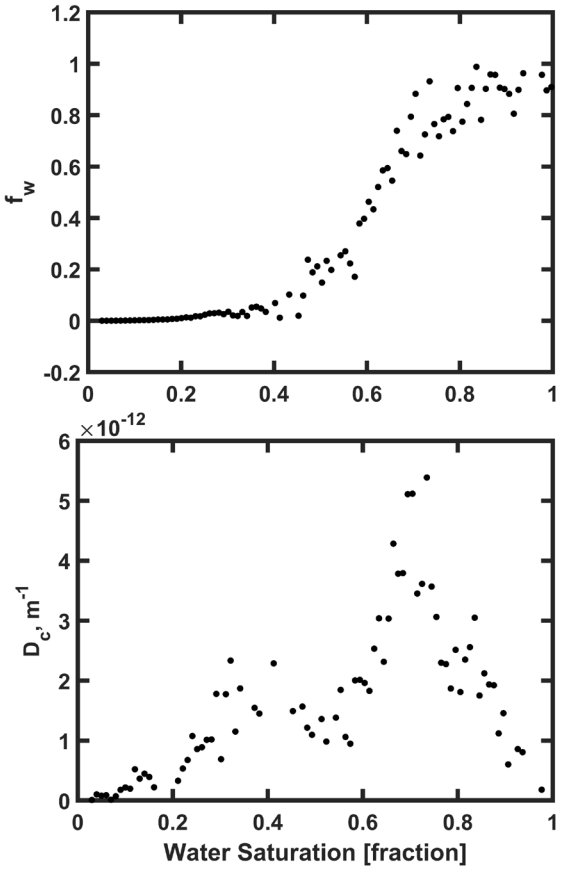

Fig. 10. Saturation dependant functions (a) $f_w(S_w)$ and (b) $D_c(S_w)$ for the drainage experiment. $f_w(S_w)$ and $D_c(S_w)$ were calculated using Eq. 9 and employing derivative of saturation with respect to position and water flow rate.

Table. 6. Fitted P_c and k_r parameters.

Curves	Parameters	Proposed method	CYDAR
Relative permeability parameters	k_{rw}^{max}	–	1
	k_{ro}^{max}	–	1.568
	α_w	–	5.551
	α_o	–	1.7
Reduced water saturation	S_{min}	0.03	0.02
	S_{max}	1	1
Capillary pressure parameters	p_o [mbar]	2.7	7.738
	p_t [mbar]	50	50.3

Conclusion

A method is introduced to measure relative permeability curves using in situ saturation data. This approach is model-free and does not require any assumptions about the functional forms of the relative permeability curves. In this method, partial derivatives of fluid saturation are used along with the governing equations of immiscible displacement to give water fractional flow function and capillary dispersion function. These functions incorporate relative permeability terms and are only functions of fluid saturation. A parametrized capillary pressure curve was then assumed, and the pressure drop across the sample was matched by adjusting the capillary pressure parameters to derive relative permeability curves. The methodology was validated using synthetic data for drainage and imbibition processes. It was shown that it can determine relative permeability curves successfully. Furthermore, the method was applied to derive relative permeability curves for a Bentheimer core plug subjected to primary drainage. The evolution of saturation profiles was acquired using a ^{23}Na MRI method, SE-SPI. Unlike ^{1}H MRI, ^{23}Na MRI enabled the detection of the brine signal without interference from the oil phase signal. The imaging method gave quantitative saturation profiles suitable for evaluating partial derivatives. The derived relative permeabilities were compared with those obtained from conventional numerical simulation using production and pressure drop data.

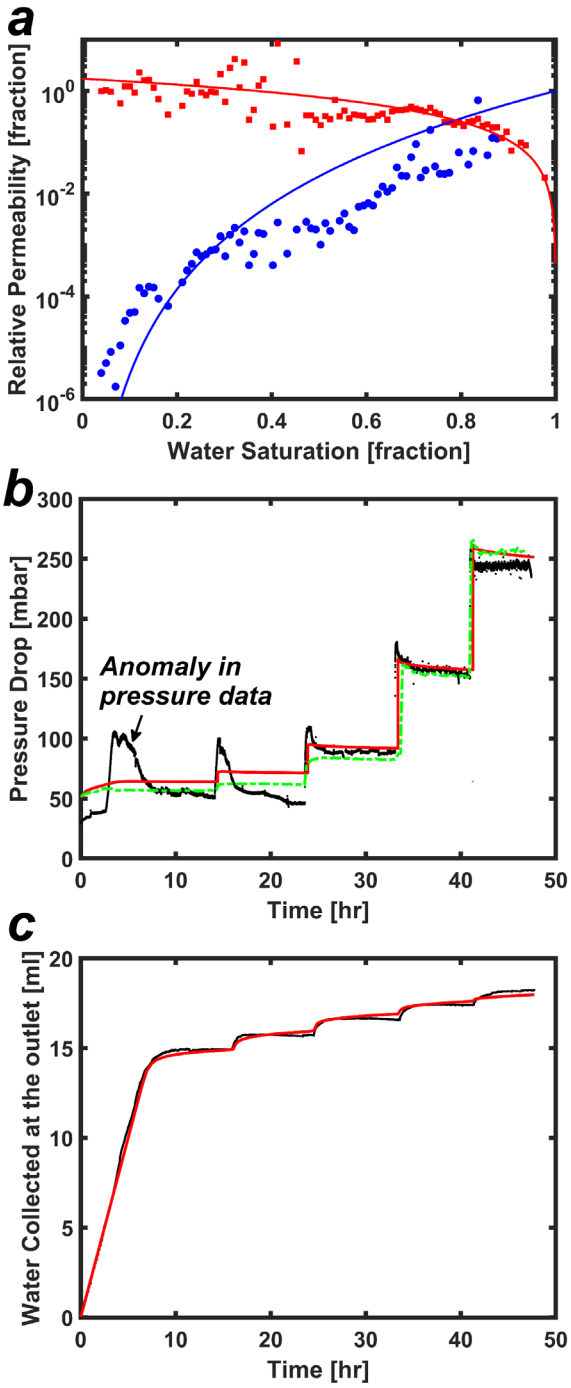

Fig. 11. (a) Relative permeability curves of oil and water phases derived using in-situ saturation tracking method. The continuous curves are relative permeability curves fitted by CYDAR software. Red and blue colors represent oil and water phases, respectively. (b) Black data points are pressure drop measured across the core plug. The green dashed line is the pressure drop calculated using solution of Eq. 14 with relative permeability data points given in Figure 11a and capillary pressure parameters given in Table 6. The continuous red line is CYDAR fit. (c) The black line is the measured water volume collected at the outlet, and the red line is the fit by CYDAR. The dead volume at the outlet was 6.52 ml.

Appendix A

For a the saturation profile, $S_w(x)$, knowing the relative permeability curves, k_{rw} and k_{ro}, and capillary pressure,

P_c, the pressure equation given by Eq. 14 can be solved to give pressure profiles, P. The linearized from of the Eq. 14 is given by Eq. A1 [29].

$$\mathbf{T}\,\mathrm{P} = \mathrm{b} \tag{A1}$$

Where matrix $\mathbf{T} \in \mathbb{R}^{n_x-1 \times n_x-1}$ contains transmissibility terms, $T_o = KA\,k_{ro}$ and $T_w = KA\,k_{rw}$. The vector $\mathrm{b} \in \mathbb{R}^{n_x-1}$ is defined as below:

$$\mathbf{T} = \begin{bmatrix} -\left(\mathrm{T}_{\mathrm{o}_{1+\frac{1}{2}}} + \mathrm{T}_{\mathrm{w}_{1+\frac{1}{2}}}\right) & \mathrm{T}_{\mathrm{o}_{1+\frac{1}{2}}} + \mathrm{T}_{\mathrm{w}_{1+\frac{1}{2}}} & 0 & \cdots & 0 \\ \mathrm{T}_{\mathrm{o}_{2-\frac{1}{2}}} + \mathrm{T}_{\mathrm{w}_{2-\frac{1}{2}}} & -\left(\mathrm{T}_{\mathrm{o}_{2-\frac{1}{2}}} + \mathrm{T}_{\mathrm{o}_{2+\frac{1}{2}}} + \mathrm{T}_{\mathrm{w}_{2-\frac{1}{2}}} + \mathrm{T}_{\mathrm{w}_{2+\frac{1}{2}}}\right) & \mathrm{T}_{\mathrm{o}_{2+\frac{1}{2}}} + \mathrm{T}_{\mathrm{w}_{2+\frac{1}{2}}} & & \\ & \vdots & & \ddots & \vdots \\ 0 & 0 & 0 & \cdots & \end{bmatrix}$$

$$\mathrm{b} = \begin{bmatrix} \mathrm{T}_{\mathrm{w}_{1+\frac{1}{2}}}\left(\mathrm{P}_{\mathrm{c}_2} - \mathrm{P}_{\mathrm{c}_1}\right) - \mathrm{q}_{\mathrm{oi}} \\ \mathrm{T}_{\mathrm{w}_{2-\frac{1}{2}}}\left(\mathrm{P}_{\mathrm{c}_1} - \mathrm{P}_{\mathrm{c}_2}\right) + \mathrm{T}_{\mathrm{w}_{2+\frac{1}{2}}}\left(\mathrm{P}_{\mathrm{c}_3} - \mathrm{P}_{\mathrm{c}_2}\right) \\ \vdots \\ \mathrm{T}_{\mathrm{w}_{\mathrm{nx}-1-\frac{1}{2}}}\left(\mathrm{P}_{\mathrm{c}_{\mathrm{nx}-2}} - \mathrm{P}_{\mathrm{c}_{\mathrm{nx}-1}}\right) + \mathrm{T}_{\mathrm{w}_{\mathrm{nx}-1+\frac{1}{2}}}\left(\mathrm{P}_{\mathrm{c}_{\mathrm{nx}}} - \mathrm{P}_{\mathrm{c}_{\mathrm{nx}-1}}\right) - \left(\mathrm{T}_{\mathrm{w}_{\mathrm{nx}-1-\frac{1}{2}}} + \mathrm{T}_{\mathrm{w}_{\mathrm{nx}-1+\frac{1}{2}}}\right).\mathrm{P}_{\mathrm{e}} \end{bmatrix}$$

$$\mathrm{P} = \begin{bmatrix} \mathrm{P}_1 \\ \mathrm{P}_2 \\ \vdots \\ \mathrm{P}_{\mathrm{n_x}-1} \end{bmatrix}$$

where $\mathrm{P_e}$ is the pressure at the outlet of the core plug, $\mathrm{q_{oi}}$ is injection rate at the inlet. The numerical indices indicates position.

Authors acknowledge TotalEnergies and Green Imaging Technologies for financial support. We thank the Canada Chairs program for a Research Chair in Material Science MRI [950-230894] and an NSERC Alliance award grant [ALLRP 571885-21]. S. Zamiri would like to thank Armin Afrough for valuable discussions and recommendations on data analysis.

References

1. R.L. Christiansen, *Two-Phase Flow Through Porous Media: Theory, Art and Reality of Relative Permeability and Capillary Pressure*, (Colorado School of Mines, Colorado, (2001).
2. C. McPhee, J. Reed, I. Zubizarreta, *Core Analysis: A Best Practice Guide* (Elsevier, Amsterdam, 2015)
3. H. R. Warner, *The Reservoir Engineering Aspects of waterflooding*, SPE, Richardson, (2015).
4. T.M. Geffen, W.W. Owens, D.R. Parrish, R.A. Morse, J Pet Technol **3**, 99–110, (1951).
5. W. Anderson, J. Pet. Technol. 39, 1283–1300 (1987)
6. M. Yaralidarani, H. Shahverdi, J. pet. explor. prod. technol. **8**,1559–1572, (2018).
7. S. Berg, H. Dijk, E. Unsal, R. Hofmann, B. Zhao, V.R. Ahuja, Comput. Geotech. 168, 106091, (2024).
8. S.K. Masalmeh, T.G. Sorop, B.M.J.M. Suijkerbuijk, E.C.M. Vermolen, S. Douma, H.A. van der Linde, S.G.J. Pieterse, IPTC 17558, *International Petroleum Technology Conference*, (2014).
9. A. Almutairi, F. Othman, J. Ge, F. Le-Hussain, J. Pet. Sci. Eng. **210**, 110064, (2022).
10. G. Zhang, S. Foroughi, B. Bijeljic, M.J. Blunt, Transp. Porous Media **149**, 837–852, (2023)
11. C. Chardaire-Riviere, G. Chavent, J. Jaffre, J. Liu, B. Bourbiaux, SPE Form Eval. **7**(04), 283-289, (1992).
12. G. Mejia, K. Mohanty, A. Watson, J. Pet. Sci. Eng. **12**, 233-245, (1995).
13. H. Ott, C.H. Pentland, S. Oedai, Int. J. Greenhouse Gas Control **33**, 135-144, (2015).
14. P. Naylor, N. Sargent, A. Crosbie, A. Tilsed, S. Goodyear, *Pet Geosci.*, **2**, 69-74, (1996).
15. P. Richmond, A. Watsons, *SPE Res Eng.*, **5**, 121-127, (1990).
16. A.E. Fincham, B. Ferreol, SPE-50576-MS, *European Petroleum Conference,* (1998).
17. R. Lenormand, K. Lorentzen, J.G. Maas, D. Ruth, *Petrophysics* **58**(1) 48-56, (2017).
18. J.G. Maas, B. Flemisch, A. Hebing, "*Open source simulator DuMux available for SCAL data interpretation*", SCA 2011-08, (2011).
19. R.H. Brooks, A. Corey, Hydrological Papers, Colorado State University (1964)
20. A.T. Corey, *The interrelation between gas and oil relative permeabilities*. Prod. Monthly. **19**, 38–41. (1954).
21. M. Goodfield, S.G. Goodyear, P.H. Townsley, SPE-71490-MS, *SPE Annual Technical Conference and Exhibition,* (2001).
22. H. Kusanagi, N. Watanabe, T. Shimazu, Y. Masahiko, *SPWLA 22nd Formation Evaluation Symposium of Japan,* (2016).
23. N. Ansaribaranghar, M.S. Zamiri, L. Romero-Zerón, F. Marica, A. Ramirez, D. Green, B. Nicot, B.J. Balcom, Paper SCA-2023-018, *International Symposium of the Society of Core Analysts,* (2023).
24. N. Ansaribaranghar, M.S. Zamiri, L. Romero-Zerón, F. Marica, A. Ramirez, D. Green, B. Nicot, B.J. Balcom, Paper SCA-2023-005, *International Symposium of the Society of Core Analysts,* (2013).
25. L.P. Dake, *Fundamentals of Reservoir Engineering* Elsevier, (1978).
26. M. Sahimi, *Rev Mod Phys.* **65**, 1393-1534 (1993)
27. C. Shen, D.W. Ruth, J Can Pet Technol. **35**, PETSOC-96-01-03, (1996).
28. C. Shen, D.W. Ruth, Transp. Porous Media **16**, 105–123, (1994).
29. T. Ertekin, J.H. Abou-Kassem, G.R. King, *Basic Applied Reservoir Simulation* (SPE, 2001)
30. C.E. Muir, B.J. Balcom, Ann R NMR S **77**, 81-113, (2012).
31. O. Petrov, G. Ersland, B.J. Balcom, J Magn Reson, **209**, 39-46, (2011).